

See discussions, stats, and author profiles for this publication at: <https://www.researchgate.net/publication/263952680>

Pluronic Micellar Aggregates Loaded with Gold Nanoparticles (Au NPs) and Fluorescent Dyes: A Study of Controlled Nanometal Surface Energy Transfer

ARTICLE *in* THE JOURNAL OF PHYSICAL CHEMISTRY C · FEBRUARY 2012

Impact Factor: 4.77 · DOI: 10.1021/jp2093127

CITATIONS

22

READS

70

5 AUTHORS, INCLUDING:



Sarthak Mandal

Columbia University

44 PUBLICATIONS 444 CITATIONS

[SEE PROFILE](#)



Chiranjib Ghatak

University of Kansas

38 PUBLICATIONS 570 CITATIONS

[SEE PROFILE](#)



Vishal Govind Rao

Bowling Green State University

49 PUBLICATIONS 533 CITATIONS

[SEE PROFILE](#)



Nilmoni Sarkar

IIT Kharagpur

159 PUBLICATIONS 3,689 CITATIONS

[SEE PROFILE](#)

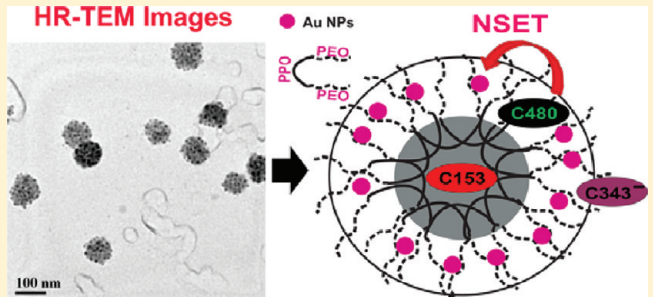
Pluronic Micellar Aggregates Loaded with Gold Nanoparticles (Au NPs) and Fluorescent Dyes: A Study of Controlled Nanometal Surface Energy Transfer

Sarthak Mandal, Chiranjib Ghatak, Vishal Govind Rao, Surajit Ghosh, and Nilmoni Sarkar*

Department of Chemistry, Indian Institute of Technology, Kharagpur 721302, WB, India

Supporting Information

ABSTRACT: In this work we have reported the controlled synthesis of gold nanoparticles into the surface cavities of P123 micellar assemblies together with the fluorescent dye molecules and investigated nanometal surface energy transfer (NSET) from confined donor dye to metal nanoparticles. The formation of hybrid spherical assemblies of P123 combined with fluorescent dyes and gold nanoparticles has been confirmed from HR-TEM, DLS, UV-vis, and fluorescence spectroscopic studies. The observed steady state as well as time-resolved fluorescence quenching of the confined micellar dyes present in the close proximity of gold nanoparticles which are attached to the surface of micellar assemblies, indicates efficient surface energy transfer from dye to gold (Au) nanoparticles. Since the NSET process is strongly dependent on the distance between donor dye and acceptor nanoparticles, successful applications of NSET require the perfect control over their relative location. Herein, we investigate the utilization of nanoparticles embedded self-assemblies of P123 for controlled NSET by tuning the precise location of donor dyes. Through the nanoencapsulation of the different fluorophore having different location inside P123 micelles, we have shown the corona region of P123 micelles as a perfect place for NSET and the core region as a barrier for NSET. Additionally, we have investigated the microenvironment of the confined micellar probe molecules in presence and absence of nanoparticles. This study further reveals that when the system changes from normal micelles to nanoparticles loaded hybrid micelles, unlike the probes C480 and C153, the anionic probe C343 undergoes a change in its location indicating the modulation of the properties of micelles in presence of nanoparticles.



INTRODUCTION

In recent years, there has been a great deal of interest among researchers in the use of amphiphilic triblock copolymer (TBP) systems to build a wide variety of applications, such as chemical, biological and industrial applications.^{1–3} The most widely studied poly(ethylene oxide)-*b*-poly(propylene oxide)-*b*-poly(ethylene oxide) (PEO-*b*-PPO-*b*-PEO), pluronic TBPs are commercially available over a range of molecular weight with different composition of hydrophilic (polyethylene oxide, PEO) and hydrophobic (polypropylene oxide, PPO) blocks.⁴ Because of the stability, chemical and structural diversity, controllable molecular weight, useful mechanical properties, and most importantly their environmentally friendly nontoxic nature, pluronic TBPs have been used extensively to prepare various self-assembled biomimicking organized structures like micelles, mixed micelles,⁵ and vesicles (polymersomes),⁶ depending on the experimental conditions like temperature, concentration, composition and solubilizing media for various applications. These confined model systems are now being applied in medicinal chemistry as vehicles of drug carrier,¹ catalytic reaction media,⁷ and templates for nanoparticles synthesis.^{8,72}

Many efforts have been made in order to understand the structural and conformational dynamics of the different

nanostructures of block copolymers using different ultrafast fluorescence studies^{32,58,59} like fluorescence resonance energy transfer (FRET),⁹ solvation and rotational dynamics, photo-induced electron transfer, fluorescence correlation spectroscopy,¹⁰ etc. Among these fluorescence based applications, fluorescence resonance energy transfer (FRET) between molecular donor and acceptors, as well as other resonance energy transfer processes have been extensively studied for decades to probe the structure and dynamics of many complex biological systems.^{11–15} FRET is used as a powerful optical tool for the determination of the distances between donor and acceptor mostly when they are covalently labeled at the two specific sites of a rigid biological macromolecule, for example, rigid biopolymers.^{11–15,31} However, it has also been used to probe the structural changes of the biological relevant systems like micelles, vesicles, etc. where the actual donor–acceptor distance is not being measured.^{32,33} Such studies help to understand the extent of binding of the systems even though the actual distance is not known.¹⁵ Although FRET is a very

Received: September 27, 2011

Revised: February 6, 2012

Published: February 7, 2012



effective and convenient technique and can be applied at single molecule detection limit known as smFRET,¹⁶ but it has serious limitations regarding the distance and orientation of donor and acceptor.¹⁸ FRET is restricted to determine the distance up to the separation of only 80 Å. To overcome these limitations, utilization of unique optical properties of gold nanoparticles as universal acceptor in the study of nanometal surface energy transfer (NSET) from molecular donor to metal nanoparticles has recently been developed.^{12–14,17–23} Very recently, with the development of quantum dots (QDs),²⁴ utilization of QDs as tunable donors in the QD-based fluorescence resonance energy transfer^{25–29} has also been paid a great attention because of their tunable spectral range over the dye molecules.³⁰ NSET study allows determining the distance nearly twice than that obtained from FRET and thus helps to understand the long-range conformational changes of many complex macromolecules where FRET is not operational.^{13,21} Basically, NSET is a FRET like process, which originates from the interaction of the electromagnetic field of the donor dipole with the conduction band's delocalized electrons of acceptor, but the fundamental difference is that, unlike FRET, NSET does not require a resonant electronic transitions.³⁴

Interaction with the metal nanoparticles may either leads to radiative quenching as a result of NSET or radiative enhancement depending on the nature of coupling between the surface plasmon resonance (SPR) oscillation and dye molecules as empirically described by Lakowicz.^{35,36} According to radiating plasmon (RP) model proposed by Lakowicz the quenching occurs due to the absorption component present in the extinction spectra while the enhancement arises from the scattering contribution. Jain et al.³⁷ using Mie theory³⁸ and the discrete dipole approximation (DDA)³⁹ method calculated absorption and scattering contribution of gold nanoparticles of different size, shape, and composition. Moreover, the size, shape and chemical composition of the nanoparticles strongly influence their optical properties as described by Schatz et al.⁴³ and hence these are the factors responsible for dictating the process of NSET.^{40–42} Considerable progress on NSET has been made experimentally^{12–14,17–23,45–47} as well as theoretically^{40–42,44} by several groups over the past few years. In most of the experimental studies they have used either DNA^{12–14,17,18} or RNA^{21–23} as linkers to establish its better applicability over the conventionally used FRET as an optical nanoruler in real biological systems as well as in the biological relevant systems. Recently, Ray et al.²¹ have demonstrated size and distance dependent NSET for selective sensing of hepatitis C virus RNA. Chen et al.¹⁹ investigated NSET as an optical ruler for the measurement of binding site distances on live cell surfaces. Since block copolymer can offer precise control over the size, shape and chemical properties of nanoparticles with the structural transitions of self-assemblies like, micelles to vesicles, which are in turn controlled by the variation of temperature, concentration and ratios of hydrophilic and hydrophobic blocks, they are a promising candidate for nanotechnological and biomedical applications.^{8,48,49} Liu et al.⁵⁰ have recently shown that amphiphilic block copolymer micelles loaded with anticancer drug and surface embedded super paramagnetic iron oxide nanoparticles are very useful for integrated chemotherapeutic drug delivery and MR Imaging. Noble metal nanoparticles, especially gold NPs, have always been in great interest for biological applications.⁵¹ Bioconjugate of gold nanoparticles, for example, DNA-Au NPs bioconjugate

can be utilize for targeted drug delivery, CT imaging, and therapy for prostate cancer.^{52,53} As it is well established that self-assemblies of pluronic TBPs are a promising candidate for drug delivery,^{1,54,55} in situ synthesis of gold nanoparticles into the surface cavities of drug loaded micelles could be very useful for nanotechnological cum biological applications. The motivation of the present study is to establish a new type of plasmonic nanohybrids⁵⁶ with Au NPs and fluorescent dyes, which could allow the utilization of plasmon coupled optical properties such as, NSET to pave a way toward their greater applicability in sensing, nanophotonics and biological applications.

Recent investigations have shown that self-assemblies of block copolymers are very useful for controlled FRET enabling the accurate positioning of the multiple fluorophore.^{57–59} Tong et al.⁹ demonstrated that micellar assemblies of triblock copolymer in water can serve as a novel scaffold for FRET. While substantial effort has been made on the study of FRET using pluronic micelles as biological model system,^{32,60} there is no report on the study of NSET from a stable pluronic micellar dye (dye loaded micelles) to the gold nanoparticles which are being synthesized and stabilized in situ together with the dye molecules. Regarding the NSET in aqueous solution of polymer, very recently, B. Karthikeyan⁶¹ has investigated SET leading to quenching of Rh6G in Au Nanocomposite of polymer, polyvinyl alcohol (PVA), but not with stable hydrophobic pluronic TBPs forming micelles as biological model system which does not break during and after the synthesis of nanoparticles and where both the dye molecules and nanoparticles are confined. Successful application of NSET between donor and acceptor requires precise control over their relative position and involvement of spectral overlap between fluorescence of donors and surface plasmon resonance band of acceptor NPs. Therefore, in the present work successful effort has been made to synthesize gold nanoparticles of average diameter ~8–10 nm into the surface cavities of fluorescent dye loaded P123 micelles at 25 °C, for controlled NSET study using steady state and time-resolved fluorescence measurements. Finally, using different dye molecules having different location inside micelles, we have shown the enabling and restriction of NSET in Au–P123 hybrid nanospheres.^{58,59} From the steady state and time-resolved experiment we can establish the concept that nanoencapsulation of fluorophores and nanoparticles into the same corona region of P123 micelles allowed effective dye to nanometal surface energy transfer and thus can be a suitable place for NSET. However, the dye molecules present in the core are far apart from the surface embedded nanoparticles in Au–P123 nanohybrid and hence hydrophobic core region acts as an effective barrier for NSET. Additionally, we have also investigated the change in the microenvironment of the micellar probe molecules both in the presence and absence of nanoparticles from the steady state and time-resolved observations. The most interesting observation is that, the presence of nanoparticles inside P123 micellar assemblies helps to drag negatively charged probe molecules like Coumarin 343 (C343) from aqueous micellar surface to the interior and thus modifying the properties of micelles.^{62–64}

EXPERIMENTAL SECTION

Materials. Laser grade coumarin 153 (C153), coumarin 480 (C480), coumarin 343 (C343), and rhodamine 6G (Rh6G) were purchased from exciton. The chemical structures of all of the dyes are given in Supporting Information (Scheme-1). The

triblock copolymer P123 was obtained from Sigma Aldrich and used as received to prepare micellar solution. Hydrogen tetrachloroaurate (III) hydrate ($\text{HAuCl}_4 \cdot 3\text{H}_2\text{O}$) was also obtained from Sigma Aldrich.

Preparation of Dye Loaded Micelles. For the preparation of aqueous solution of dye loaded micelles, we first prepared 5 wt % stock solution of P123 by mixing (stirring with a magnetic stirrer) appropriate amount of copolymer with 50 mL water in a sealed container at room temperature. The solution was kept overnight under refrigeration for stabilization. Now calculated amount of stock methanolic solution of dye was taken in a volumetric flask so that ultimate concentration becomes 2×10^{-6} (M) for a specific volume of P123 micellar solution. After removing methanol completely, specific volume of stock micellar solution was added into the flask and the solution was kept for few hours for the encapsulation of dye into the microenvironment of micelles.

Synthesis of Au Nanoparticles inside the Dye Loaded Micelles. For the preparation of gold nanoparticles into the surface cavities of stable P123 micelles in presence or absence of organic dye, the required amount of stock aqueous solution of $\text{HAuCl}_4 \cdot 3\text{H}_2\text{O}$ (20 mM, 20 μL) was added dropwise to the stock dye loaded or dye free micellar solution of P123 (5 wt %, 2 mL) on a magnetic stirrer at 25 °C temperature. After complete addition, the stirring was stopped and the solution was kept undisturbed for 1 h. The color of the solution gradually changes from colorless to red pink within half an hour.

Optical Characterization. UV-vis measurements were carried out at different time interval to follow the progress of reaction with time using Shimadzu (model UV 1601) UV-vis spectrophotometer. The absorption coefficients required for the estimation of spectral overlap between donor emission and the acceptor absorption were calculated from Beer's law using an estimated concentration of nanoparticles. The number of nanoparticles in a particular solution was determined from the total mass of the metal taken divided by mass of individual spherical metal nanoparticles whose average radius was obtained from HRTEM analysis assuming the complete synthesis of Au^0 nanoparticles from Au^{3+} salt.⁶⁵ Moreover, the concentrations of gold nanoparticles at different time intervals were roughly estimated from UV-vis spectra following the literature procedure.^{18,66}

The steady state fluorescence emission spectra of the samples were recorded using Hitachi (model no. F-7000) spectrofluorimeter. The time-resolved emission spectra were recorded using TCSPC picosecond spectrophotometer. In brief, picoseconds diode laser at 440 and 410 nm (IBH, U.K., Nanoled) were used as light source and the signal was detected in magic angle (54.7°) polarization using Hamamatsu MCP PMT (3809U). The typical instrument response function is ~100 ps in our system. The time-resolved emission decays were monitored at the emission maxima of the corresponding probe molecules. The decays were analyzed using IBH DAS-6 decay analysis software.

The fluorescence quantum yield of C480, Rh6G and C343 in normal P123 micelles were determined using reported⁶⁷ quantum yield 0.66 of C480 in water, 0.95 of Rh6G in

ethanol,⁶⁸ and 0.63 of C343 in ethanol,⁶⁹ respectively as the secondary standard in the following equation

$$\frac{\Phi_S}{\Phi_R} = \frac{A_S (\text{Abs})_R}{A_R (\text{Abs})_S} \frac{n_S^2}{n_R^2} \quad (1)$$

where Φ represents quantum yield, Abs represents absorbance, A represents area under the fluorescence curve, and n is refractive index of the medium. The subscripts S and R denote the corresponding parameters for the sample and reference, respectively.

Structural Characterization. Transmission electron microscopy (TEM) analysis was carried out for the structural analysis of gold nanoparticles by using JEOL model JEM 2010 transmission electron microscope at an operating voltage 200 kV. TEM images of free micelles have been taken by using 1 wt % aqueous solution of uranyl acetate as staining agent. Dynamic light scattering (DLS) measurements were carried out to determine the size of the normal P123 micelles and nanoparticles embedded micelles using Malvern Nano ZS instrument employing a 4 mW He-Ne laser ($\lambda = 632.8$ nm) and equipped with a thermostatic sample chamber.

RESULTS AND DISCUSSIONS

Figure 1 shows the HR-TEM images of normal micelles and gold nanoparticles encapsulated hybrid micelles of P123 (5 wt

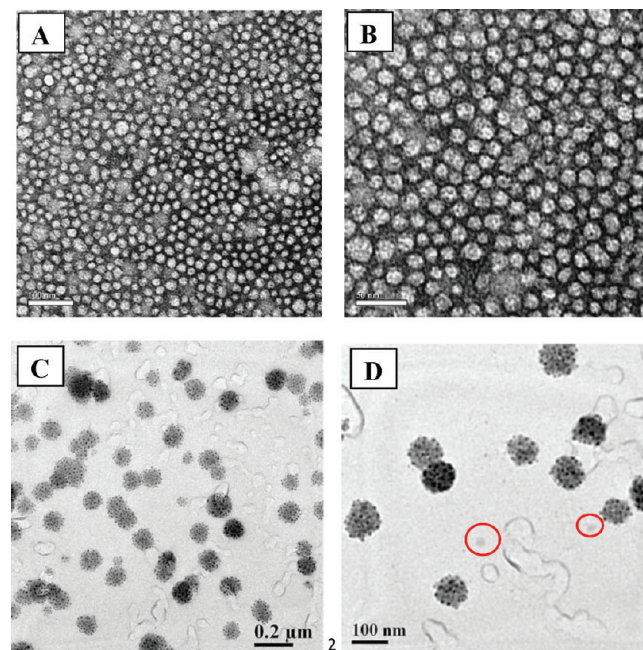


Figure 1. HR-TEM images of P123 micelles [A (scale bar represents 100 nm) and B (scale bar represents 50 nm)] and gold nanoparticles encapsulated Au-P123 hybrid micellar assemblies with increasing resolution (C and D). [Red circles indicate the presence of free micelles.]

) at 25 °C. TEM images clearly indicate the uniform distribution of dark nanoparticles into the hybrid micellar assemblies of P123. The average size of the encapsulated spherical nanoparticles is ~8–10 nm. It has been found that all the nanoparticles are successfully loaded onto the surface of spherical micellar aggregates of diameter ~60–80 nm with a regular morphology. The clear TEM images of the Au-P123

nanohybrids without using any staining agent is due to electron diffraction from the nanoparticles embedded into the PEO cavities of micellar corona region. The schematic representation of the P123 micelle loaded with metal nanoparticles in their surface cavities has been shown in Figure 2b. Additionally, in

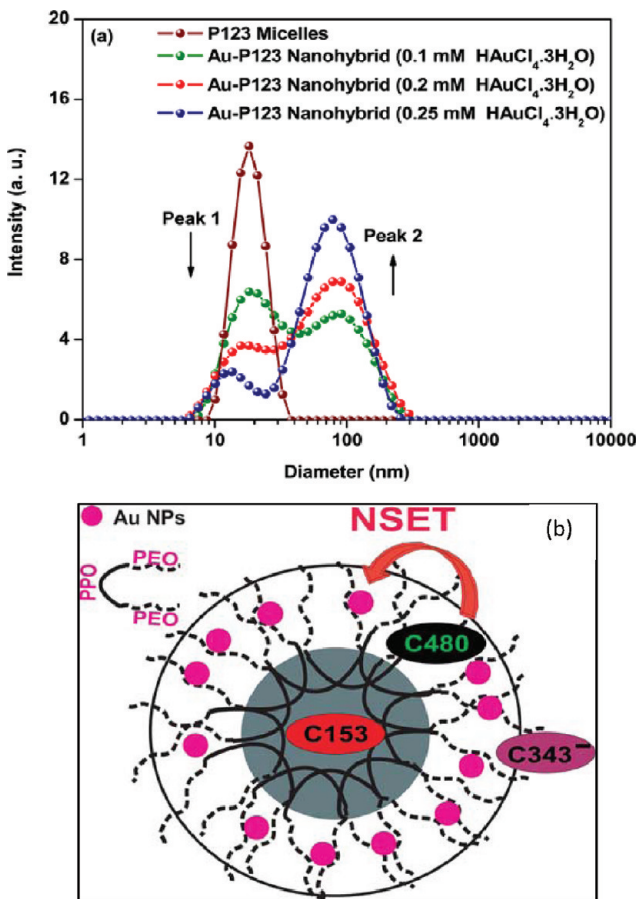


Figure 2. (a) DLS size distribution graph for normal P123 micelles (5 wt %) and Au NPs loaded hybrid micelles at varying Au NPs loading contents. (b) Schematic representation of P123 micelles with gold nanoparticles and different probe molecules having different location inside micelles.

the TEM images the nanoparticles appear to be in the whole part of the hybrid assemblies only because of the fact that TEM images are two-dimensional projections of three-dimensional assemblies.⁸ It has been well established that in P123 micelles, gold nanoparticles are typically synthesized and stabilized in situ by PEO units of hydrophilic corona region.^{48,49,72} Khuller et al.⁴⁸ have demonstrated the controlled synthesis of gold nanoparticles in the micellar solution of pluronic TBPs at different temperatures. They concluded that, stable micelles of a hydrophobic TBPs with greater number of hydrophobic PPO unit than hydrophilic PEO unit produce nanoparticles of ordered morphologies by lowering the structural transition of the micelles with the variation of temperature.⁴⁹ Their experimental evidence indicate that gold nanoparticles can only be supported by the stable hydrophobic micellar assemblies with compact arrangement of hydrophilic PEO units in the corona region. Soft micelles formed by TBPs of longer hydrophilic part than hydrophobic part produce the nanoparticles of larger in size due to the enhanced degree of hydration and the NPs are no longer supported by micellar

assemblies and hence find their way to stabilize in the bulk phase through the structural transition of micelles. However, a relatively hydrophobic triblock polymer such as, P123 which is reported to form highly stable micelles, results the formation of hybrid spherical micellar assemblies with complete coverage by gold nanoparticles as clearly observed from TEM images which are in consistent with previous literature reports.⁵⁰

To obtain further insight into the structural changes of P123 micelles due to the homogeneous incorporation of nanoparticles, we have determined the size of the aggregates using dynamic light scattering measurements. The average diameter of the normal P123 micelles is found to be ~18 nm with a narrow intensity size distribution in consistent with the reported result at 25 °C. With the homogeneous incorporation of gold nanoparticles the intensity size distribution is found to be shifted to a larger values.⁸ At low nanoparticles loading the DLS measurement exhibits dual intensity-size distribution which can be attributed to the presence of free micelles along with the nanoparticles loaded hybrid micelles into the system, because in aqueous solution of 5 wt % P123 the concentration of micelles is quite high and it is almost ~100 μM. The corresponding intensity size distribution data obtained from DLS measurement have been shown in Figure 2a. Furthermore, Figure 2A shows that when the gold nanoparticles loading content was increased gradually to 0.3 mM of HAuCl₄·3H₂O, the hydrodynamic radius distribution for free micelles (peak 1 at ~18 nm in Figure 2) disappears gradually along with the increase in intensity of the radius distribution of hybrid micelles (peak 2 at ~80 nm in Figure 2) without affecting the peak position. However, when the Au NPs content was increased to 0.35 mM of HAuCl₄·3H₂O the radius distribution for free micelles completely disappear with the appearance of a single size intensity distribution at slightly higher values. This clearly confirmed the loading of gold nanoparticles into the surface of P123 micellar assemblies to form hybrid nanospheres. As the hydrodynamic diameter increases upon formation of gold nanoparticles, a shift of the correlation function diagram is observed to a higher time scale in consistent with the literature reports.⁷⁰ The average size of the aggregates obtained from DLS measurement correlates well with the average size of the individual hybrid systems obtained from TEM images. Therefore, from the DLS measurements and TEM results we can see that the incorporation of nanoparticles into the surface cavities of P123 micelles substantially modifies the structures of P123 micelles and the size of the Au–P123 spherical aggregates are much larger than normal P123 micelles.^{5,8}

Formation of such spherical hybrid aggregates have previously been observed by Gedanken et al.⁷¹ in P123 micelles of a particular concentration of P123 using ethanol as reducing agent and lysine as an additive to stabilize gold nanoparticles onto the surface of micelles. However, it is well reported that pluronic TBPs can act as efficient reducing as well as stabilizing agent for the synthesis of gold nanoparticles. Khullar et al.^{48,49} found similar kind of gold nanoparticles embedded hybrid assemblies of relatively hydrophobic triblock copolymer P103 due to the incorporation of gold nanoparticles in situ. In the present study we have synthesized spherical hybrid aggregates in 5 wt % aqueous solution of P123 without using any further reducing or stabilizing agent. The concentration of P123 plays an important role to regulate the morphology of the aggregates.⁷¹

To demonstrate controlled NSET, a number of fluorescent dye molecules have been selected as donor on the basis of

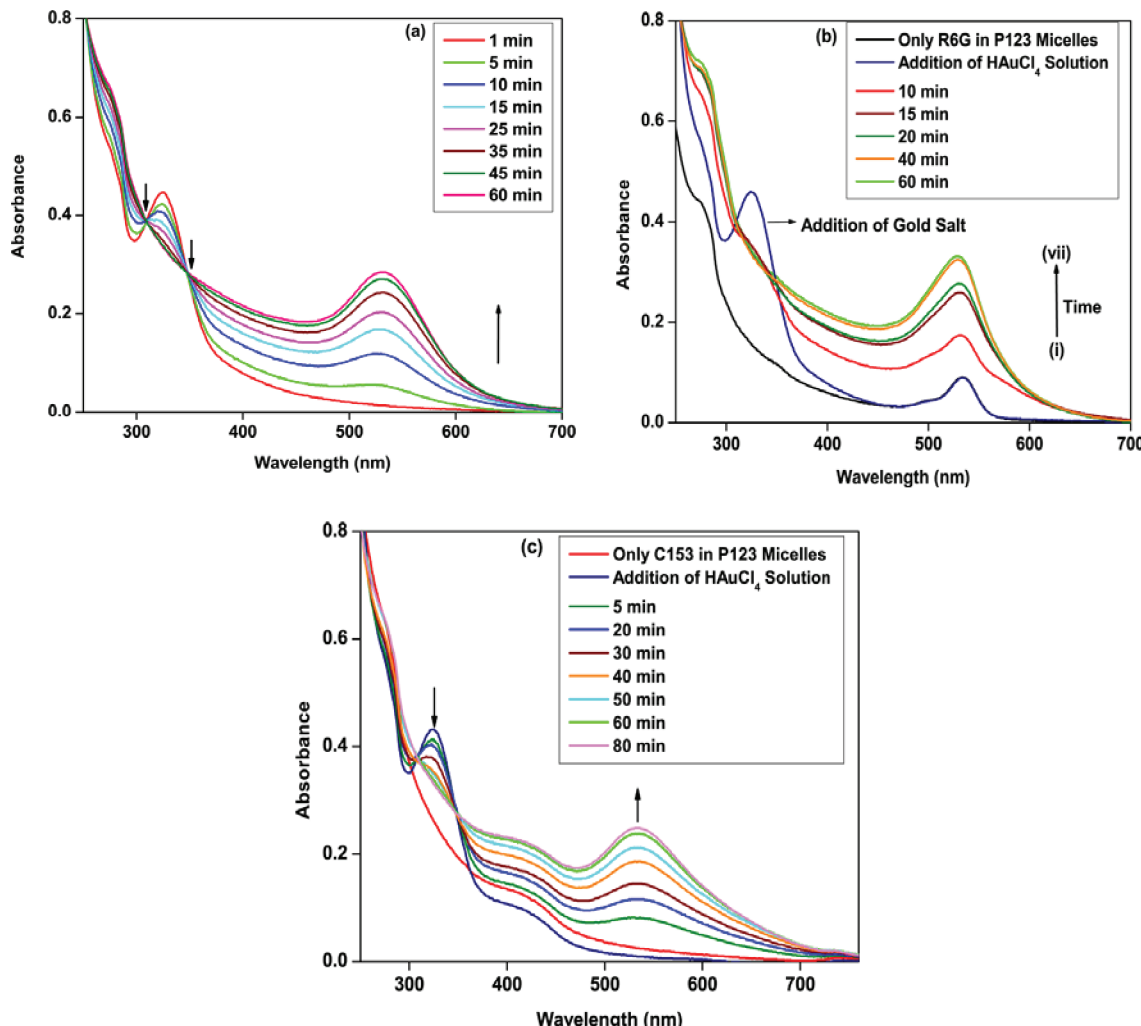


Figure 3. UV-vis. Absorption spectra recorded in different time interval to follow the synthesis of gold nanoparticles in (a) blank P123 micelles, (b) Rh6G dye loaded P123 micelles, and (c) C153 dye loaded P123 micelles.

appropriate spectral overlap between the fluorescence of donor dye and surface plasmon resonance of gold nanoparticles. The UV-vis spectra for the formation of gold nanoparticles in blank P123 micellar solution without any dye have been shown in Figure 3a. Figure 3, panels b and c, shows the UV-vis absorption spectra of Rh6G and C153 confined in the micelles and of the gold nanoparticles inside the micelles together with Rh6G and C153 dyes. The spectra were taken at different time interval to follow the reaction progress at constant temperature of 25 °C in blank P123 micellar system as well as various dye loaded micellar system. The gold nanoparticles exhibit surface plasmon resonance band at ~530 nm. An additional peak at 320 nm due to ligand to metal charge transfer (LMCT) complex appears just after addition of HAuCl₄ and disappears gradually with the reaction progress indicates the formation of nanoparticles.^{48,49} The stability of the LMCT complex in P123 micelles can be explained on the basis of the observation of isosbestic points in the UV-vis spectra during the synthesis of gold nanoparticles. This information also ruled out the structural transition like micelles to vesicles during and after the synthesis of gold nanoparticles in consistent with the earlier observations.^{48,49} The details of the UV-vis absorption spectra obtained for the synthesis of gold nanoparticles in other Coumarin dye loaded micellar environment are given in the

Supporting Information (Figure S1). A significant shift in the absorption maxima of all the dye molecules used in this experiment have been observed on efficient loading of the dyes in P123 micellar assemblies from aqueous solution. For example, the steady state absorption maximum of Rh6G in bulk water is 526 nm and this is red-shifted to 530 nm in P123 micellar system indicates efficient loading of the dye into the corona region of micelles.³² Similarly, the absorption maximum of C480 is blue-shifted ~13 nm from 396 nm in pure water to 383 in P123 micelles.³²

The steady state emission spectra of Rh6G encapsulated in the micelles and that of in the nanoparticles loaded micelles are shown in Figure 4b. A good spectral overlap (Figure 4a) between the fluorescence spectra of micellar dyes and localized surface plasmon resonance (LSPR) band of gold nanoparticles fulfill the criteria for the involvement of NSET from dye to nanoparticles.^{14,56} Before going to the details of the NSET parameters, we shed some light on the microenvironment of the probe molecules in presence and absence of nanoparticles from the steady state and time-resolved observations. The emission maximum of Rh6G is found to be red-shifted from 550 nm in bulk water to 560 nm in normal P123 micellar system.²⁹ Again, the emission maximum of Rh6G in P123 micellar environment is independent of excitation wavelength

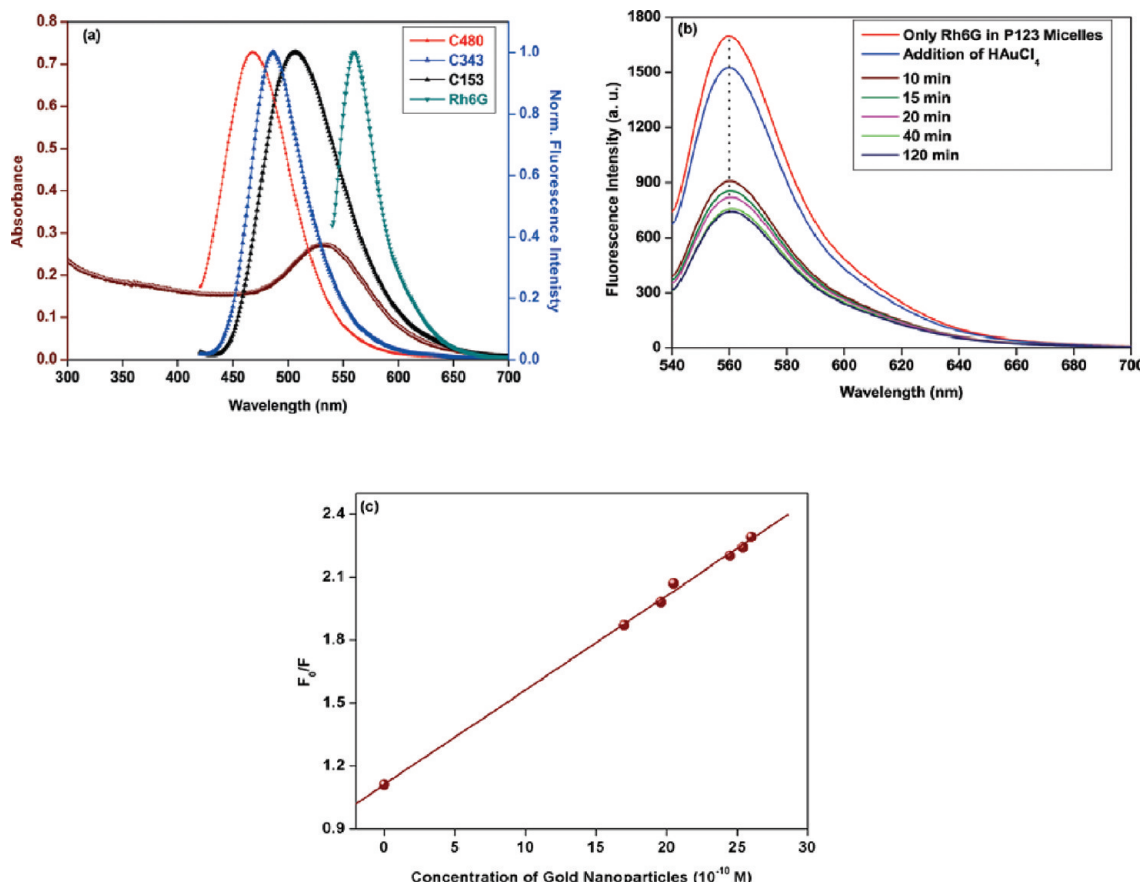


Figure 4. (a) Normalized fluorescence spectra of the donors in P123 micelles and the extinction spectra of gold nanoparticles confined in P123 micelles. (b) Steady state fluorescence quenching experiment ($\lambda_{\text{ex}} = 440$ nm) of Au NPs-P123-Rh6G hybrid assemblies at different time interval with the reaction progress. (c) Stern–Volmer plot for Rh6G in presence of Au NPs.

which indicates that location of positively charged Rh6G in P123 micelles is almost uniform and the probable location is at the hydrophilic corona region of P123 micelles.³² However, the emission maxima of Rh6G remain same both in the absence and in the presence of gold nanoparticles which is attributed to the fact that, when the system changes from normal micelles to the nanoparticles loaded hybrid micelles, Rh6G dye molecules remain confined in both the cases.^{45,46} The observed fluorescence quenching as a result of the interaction with the metal gold nanoparticles indicates efficient energy transfer between confined dye and gold nanoparticles. The steady state PL quenching efficiency of Rh6G is ~56%, obtained from the relation

$$E(I) = 1 - \frac{F}{F_0} \quad (2)$$

We have also determined the Stern–Volmer quenching constant (K_{SV}) for collisional quenching using the following Stern–Volmer relationship between the fluorescence intensity and concentration of metal nanoparticles as quencher

$$\frac{F_0}{F} = 1 + K_{\text{SV}}[Q] \quad (3)$$

where F_0 and F are the steady state fluorescence intensity in the absence and presence of quencher, respectively, and $[Q]$ is the concentration of quencher. Figure 4c shows the linear F_0/F vs $[Q]$ plot for the system where donor dye molecules are confined into the corona region of micelles and the gold

nanoparticles quenchers are homogeneously attached to the surface cavities of the corona. The K_{SV} value obtained from the slope of the linear plot is $\sim 4.5 \times 10^8 \text{ M}^{-1}$ indicating very high quenching efficiency.

Since energy transfer process is strongly dependent on the distance between donor and acceptor, successful application of energy transfer processes require precise control over their relative position. Micellar assemblies of block copolymer are very useful to achieve the precise positioning of multiple fluorophore for controlled FRET. Herein, we investigate the utilization of gold nanoparticles embedded hybrid nanostructures of P123 to demonstrate controlled NSET, using three coumarin dyes which preferably reside at the three distinct regions of P123 micelles depending on their varying hydrophobicity.⁵⁹ In P123 micelles C153 located reasonably deeper in the core region, C480 located reasonably closer to the micellar surface, and C343 located primarily in the wet phases i.e. in the aqueous micellar surface.^{58,59,62–64} Comparing the absorption and emission maxima (Table 1 in the Supporting Information) of the dye molecules in water and in P123 micelles one can confirm the efficient loading of the dye molecules in micelles. The purpose of using different dyes having different location in P123 micelles is to get a better understanding about how the energy transfer efficiencies depend on the accessibility of the dye molecules toward the quencher metal nanoparticles. The different regions of P123 micelles loaded with nanoparticles can thus be probed using steady state and time-resolved fluorescence spectroscopy. Grant

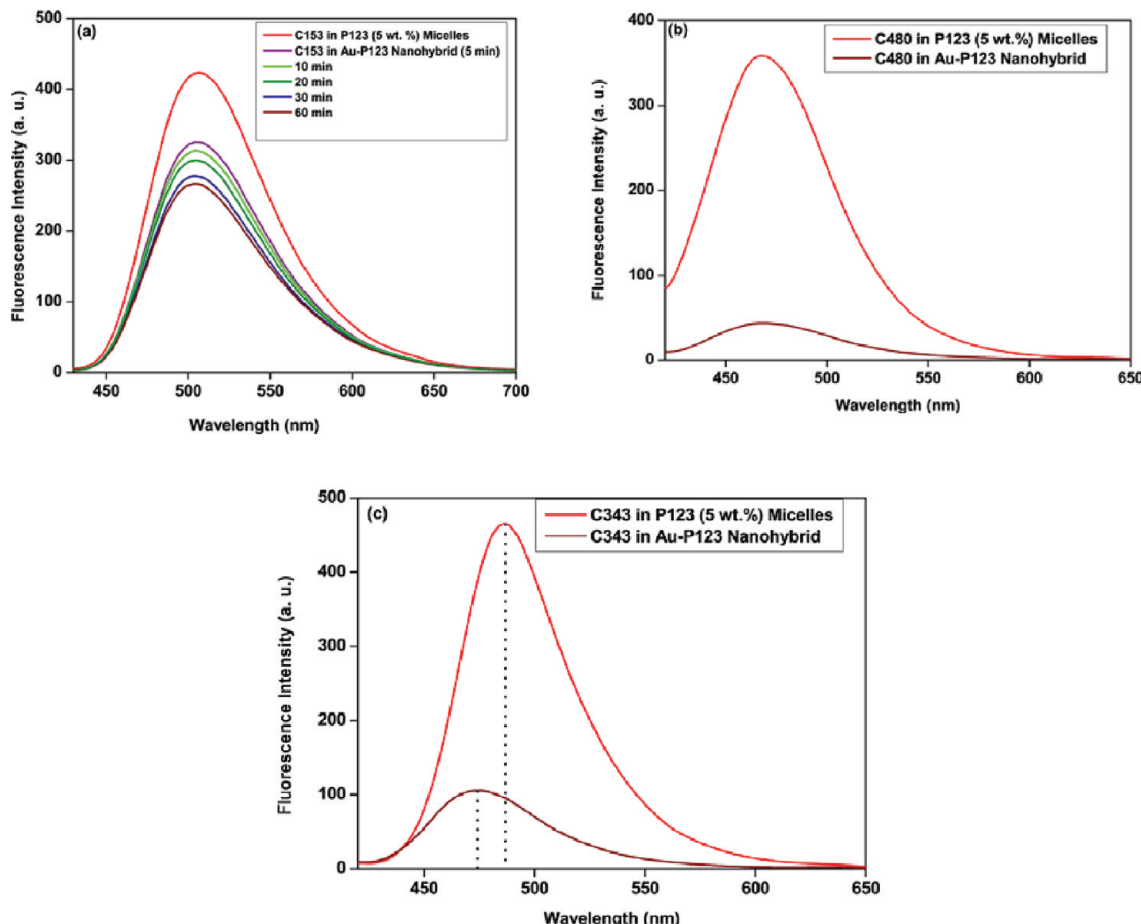


Figure 5. Steady state fluorescence quenching data for different dyes (a) C153, (b) C480, and (c) C343 in presence and absence of gold nanoparticles which are being synthesized in P123 micelles in situ. $\lambda_{\text{ex}} = 410$.

et al.^{58,59} selectively probed the different regions of various aqueous PEO-PPO-PEO triblock copolymer forming micelles using these three coumarin fluorescent probe molecules by steady state and time-resolved fluorescence spectroscopy.

The steady state emission spectra of C153, C480, and C343 encapsulated in the micelles and that of in the nanoparticles loaded hybrid micelles are shown in Figure 5. The emission maxima of C153 and C480 in P123 micelles remain almost same before and after the synthesis of gold nanoparticles, which indicates that the location of C153 and C480 inside P123 micelles remain more or less same before and after the loading of nanoparticles similar to the observation of Rh6G. However, the emission maximum of C343 is found to be blue-shifted ~ 10 nm when the system changes from normal P123 micelles to the nanoparticles loaded micelles. The results suggest that unlike the probes C480, C153, and Rh6G the anionic probe C343 undergoes a change in its location, indicating the modulation of the properties of micelles. In P123 micellar solution C343 is reported to exist in its anionic form and therefore prefer to present at the wet phase of the micellar surface.^{63,64} However, the formation of nanoparticles in the PEO cavities of micelles dragged C343 molecules into the interior of the micelles and hence the blue shift is observed. Singh et al.^{63,64} observed that addition of CTAC to the aqueous micellar solution F88 and P123 TBPs leads to the blue shift of C343 due to the incorporation into the deeper of the micelles through the interaction with the cationic headgroup of CTAC. Therefore, from the present study, we can infer that the position of a

suitable anionic probe in P123 micellar solution can be changed in presence of gold nanoparticles embedded into the nanocavity of micelles. This information could be very valuable for the application of Au–P123 hybrid nanoshperes as reaction media or in biomedical applications such as, drug delivery.

The most interesting observation is that, depending on the location of the dye molecules, the accessibility of the dye molecules toward gold nanoparticles differs and hence the extent of fluorescence quenching differs. As C153 resides reasonably deeper, probably in the core region of P123 micelles hence the accessibility of C153 toward metal nanoparticles is comparatively less than C480 and C343 which prefer to present in the corona region. This observation reflects the difference of their quenching efficiencies. The PL quenching efficiency of C153 is only 37%, while the quenching efficiency of C480 is $\sim 90\%$ and that of C343 is $\sim 77\%$. The steady-state fluorescence quenching of C153 located in the core region far away from gold nanoparticles occurs because metal nanoparticles may function as an absorber to attenuate the excitation light at the wavelength of 410 nm. Moreover the metal NPs can also function as an absorber to attenuate the emission of C153 due to the presence of good spectral overlap between the absorption band of gold NPs and steady state fluorescence emission of C153. Lim et al.⁷³ found such substantial steady-state fluorescence quenching of fluorescein ($5 \mu\text{M}$) dye in presence of HAuCl_4 and gold NPs without any chemical modification in simple aqueous solution.

Time resolved anisotropy studies shed further light on the microenvironment of probe molecules inside micelles both in presence and absence of nanoparticles. The fluorescence anisotropy decays for different coumarin dyes in P123 micellar solutions were seen to fit well with a biexponential function both in presence and absence of gold nanoparticles. The anisotropy data are given in Table 1. From the anisotropy

Table 1. Rotational Relaxation Parameter of C480 in Normal P123 Micelles and in Au NPs Loaded Spherical Hybrid Micelles

system	a_{1r}	a_{2r}	τ_{1r} (ns)	τ_{2r} (ns)	$\langle \tau_r \rangle^a$ (ns)
C480 in P123 micelles	0.53	0.47	0.306	1.99	1.10
C480 in Au-P123 hybrid spherical assemblies	0.45	0.55	0.518	2.45	1.58
C343 in P123 micelles	0.72	0.28	0.156	1.70	0.588
C343 in Au-P123 hybrid spherical assemblies	0.30	0.70	0.475	4.04	2.97

$\langle \tau_r \rangle = a_{1r}\tau_{1r} + a_{2r}\tau_{2r}$ where, τ_{1r} and τ_{2r} are two rotational relaxation time constants and a_{1r} and a_{2r} are their relative amplitude, experimental error $\pm 5\%$.

results it is evident that, when the system changes from normal micelles to the nanoparticles loaded micelles both C480, and C343 dye molecules experienced slower rotational dynamics in consistent with the literature data.⁷⁴ However, the change in average rotational relaxation time is more prominent for C343 than C480 and the observed changes in the reorientation times of C343 with the addition of HAuCl₄, not only due to presence of Au nanoparticles but rather more effective due to the change in their location from aqueous micellar surface to the interior of the micelles. On the contrary, the anisotropy decay of C153 remains unchanged before and after the nanoparticles loading. Since C153 located preferentially in the hydrophobic core of P123 micelles, far apart from the surface embedded nanoparticles hence no change is observed in the time-resolved fluorescence experiment. The anisotropy decays of different coumarin dyes in P123 micelles before and after nanoparticles loading have been shown in Figure 6. However, we did not get the well fitted anisotropy decays of Rh6G in the nanoparticles loaded micelles due to the unavoidable scattering from nanoparticles at the excitation wavelength of 440 nm.

Energy transfer processes are commonly monitored by shortening the lifetime of donor dye in presence of metal nanoparticles. Figure 7 represents the time-resolved fluorescence decay profiles of the various micellar dyes both in

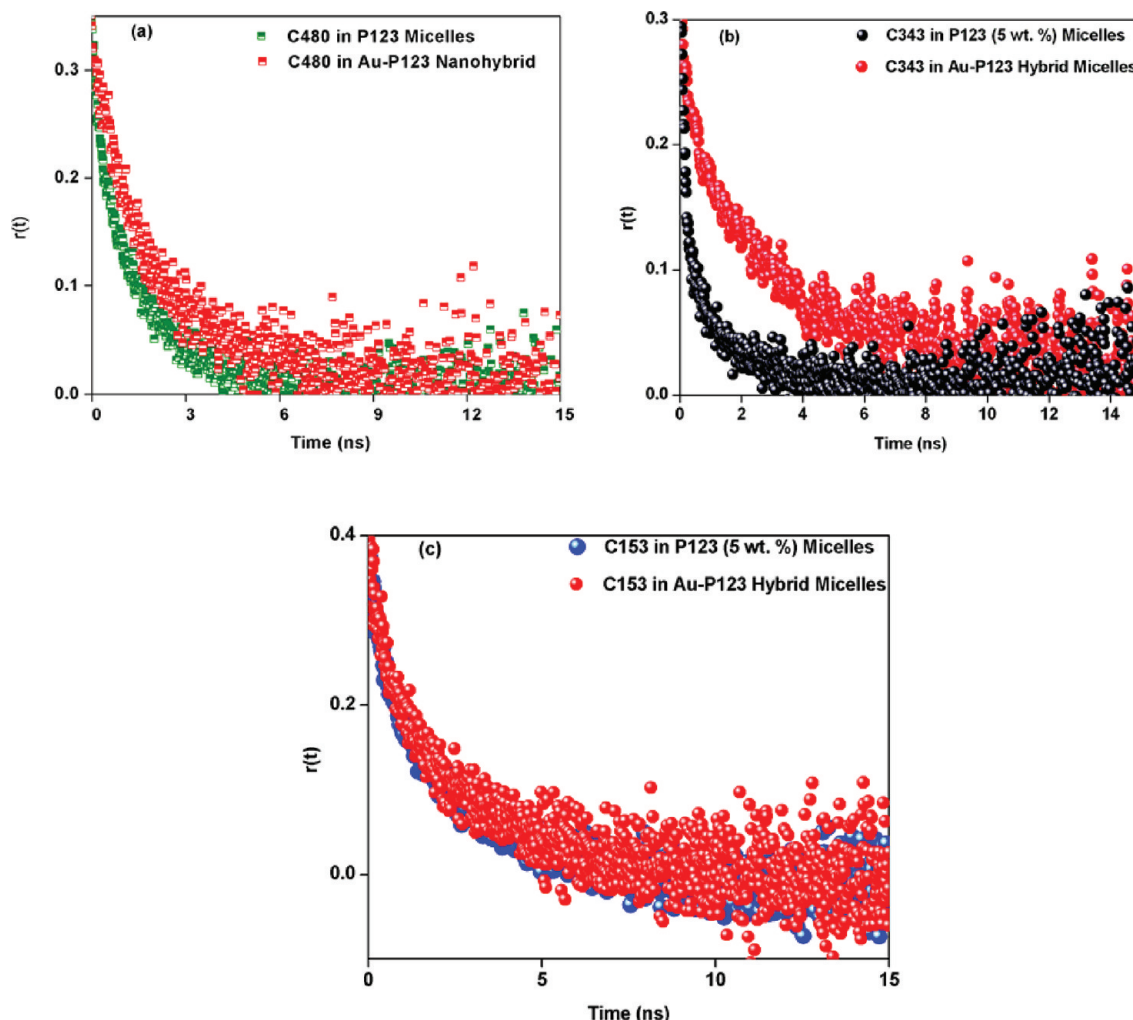


Figure 6. Fluorescence anisotropy decay of (a) C480, (b) C343, and (c) C153 in normal P123 micelles and nanoparticles loaded hybrid micelles. $\lambda_{ex} = 410$ nm.

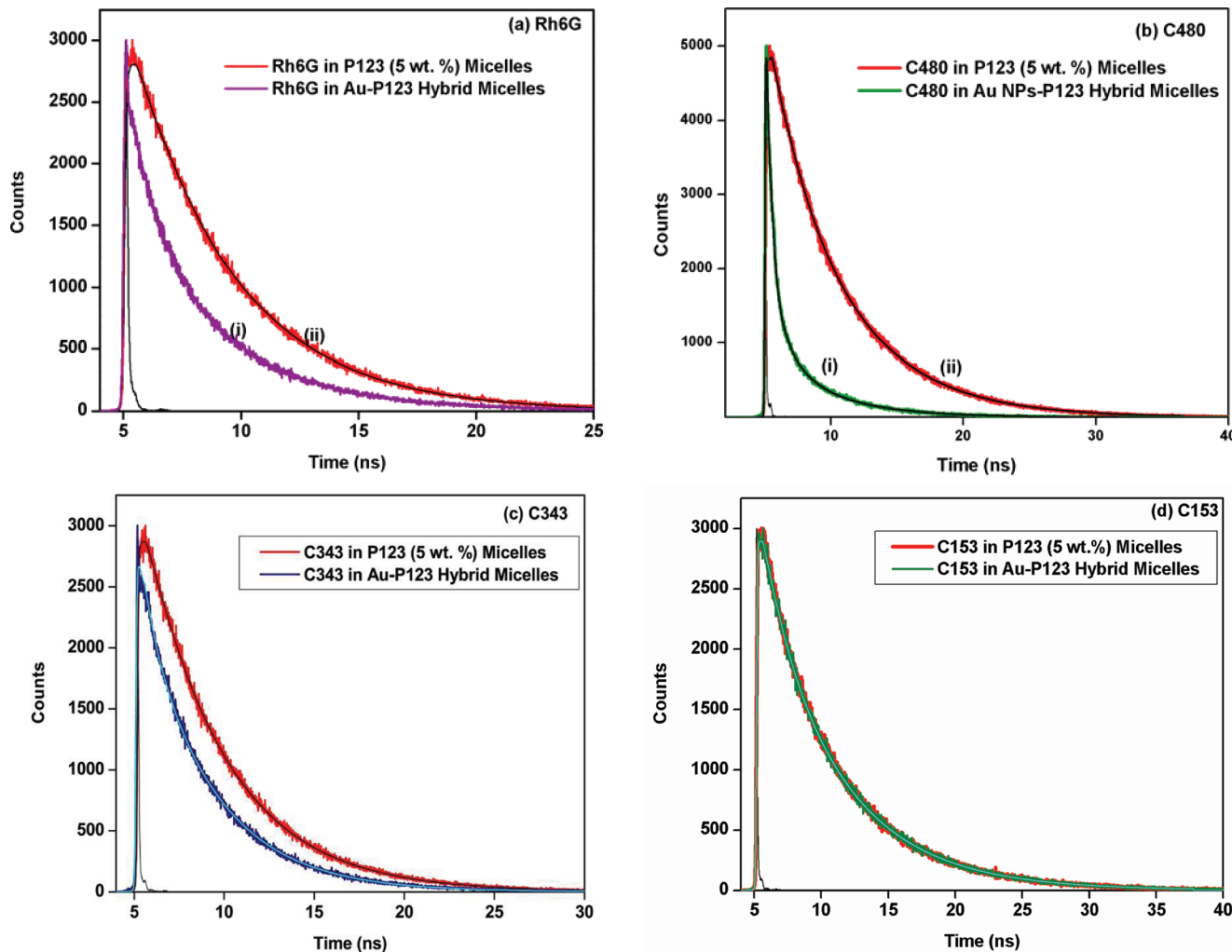


Figure 7. Time-resolved decay curves of (a) Rh6G ($\lambda_{\text{ex}} = 440$ nm and emission monitored at 560 nm), (b) C480 ($\lambda_{\text{ex}} = 410$ nm and emission monitored at 468 nm), (c) C343 ($\lambda_{\text{ex}} = 410$ nm and monitored at corresponding emission maxima), and (d) C153 ($\lambda_{\text{ex}} = 410$ nm and emission monitored at 507 nm) in normal P123 micelles and in Au NPs loaded hybrid micelles.

Table 2. Fluorescence Lifetimes and Energy Transfer Efficiencies of Different Dye-Au Systems in Confined Environment of P123 Nanohybrid

systems	a_1	τ_1 (ns)	a_2	τ_2 (ns)	a_3	τ_3 (ns)	$\tau_{\text{av}}^{\text{a}}$ (ns)	Φ_{ET} (%)
Rh6G in P123 micelles (5 wt %)				1		4.27	4.27	
Rh6G in Au-P123 nanohybrid	0.46	0.790	0.54	3.93			2.48	42
C480 in P123 micelles (5 wt %)	0.15	2.62	0.85	5.69			5.23	
C480 in Au-P123 nanohybrid	0.695	0.364	0.18	1.38	0.125	4.66	1.08	79
C343 in P123 micelles (5 wt %)			1	4.45			4.45	
C343 in Au-P123 nanohybrid	0.23	0.692	0.77	3.91			3.17	29

^a $\tau_{\text{av}} = a_1\tau_1 + a_2\tau_2 + a_3\tau_3$ for multi exponential fluorescence decays, where τ_1 , τ_2 , and τ_3 are the lifetime components with their corresponding relative amplitude a_1 , a_2 , and a_3 , experimental error $\pm 5\%$.

presence and absence of nanoparticles. The decay profiles of dyes C480 and Rh6G without intensity peak normalization have been shown in the Supporting Information (Figure. S2). From there we can get a direct evidence of decrease in the radiative decay rate, because intensities of the Au-dye fluorescence decay at $t = 0$ are a direct measure of the radiative molecular decay rates. The corresponding lifetime values obtained from the exponential fitting of the decays are given in Table 2. The time-resolved emission decay of C480 in aqueous solution of P123 fits well to a biexponential function with the time constants 2.62 ns (15%) and 5.69 ns (85%), while

in presence of nanoparticles the decay fits well with triexponential function having the time constant values 364 ps (69.5%), 1.38 ns (18%), and 4.66 ns (12.5%). Both the fast and slow components are found to be affected by nanoparticles in consistence with the previous literature reports.^{45–47} The slow and fast decay components of C480 in normal P123 micelles arise due to the fact that distribution of C480 in corona region of P123 micelles is not uniform, as indicated by 24 nm red edge excitation shift (REES) from 447 nm at $\lambda_{\text{ex}} = 335$ to 471 nm at $\lambda_{\text{ex}} = 445$ nm.³² The excitation wavelength dependent change in the emission maximum is known as

REES. When the location of a probe molecule in P123 micelles is not uniform, excitation at the blue end select those probe molecules which preferentially reside in the relatively nonpolar region (core region of PPO blocks), while excitation at the red end exclusively excite the probe molecules residing in the polar region (corona region of PEO blocks) and as a result a red shift in the emission maximum is observed upon red edge excitation. It is very well-known that in a such kind of systems where the donor–acceptor distance is not fixed, presence of nanoparticles may results complex behavior of fluorescence decays as it has been observed for all the dyes (except C153) in Au–P123 hybrid systems. Only for C153 molecules, no change in the time-resolved decay profile has been observed, which is in good agreement with the steady state fluorescence and time-resolved anisotropy experiment. For Rh6G and C343 the single exponential fitting of the decays in normal P123 micelles become biexponential in nature on nanoparticles loading. In the complex situation where there is a distribution of donor–acceptor distances, it is better to use average lifetime in the measurement of energy transfer efficiencies. The average decay time of the dye molecules in the presence and absence of surface attached Au NPs are given in Table 2. A shortening of the average lifetime was clearly observed for the dyes C480, Rh6G, and C343 in P123 micelles after loading gold nanoparticles in situ. The lifetime quenching data is assumed to be more accurate to determine the energy transfer efficiency than the steady state fluorescence intensity quenching data. The equation

$$\phi_{\text{ET}} = 1 - \frac{\tau_{\text{DA}}}{\tau_{\text{D}}} \quad (4)$$

where τ_{DA} is the lifetime of the dye in presence of Au nanoparticles and τ_{D} corresponds to the lifetime of the dye in absence of nanoparticles, is used to calculate the time-resolved energy transfer efficiencies for the dyes in Au–P123 nano-hybrid micellar system. The calculated energy transfer efficiency from micellar dye to Au nanoparticles is ~79% for C480, ~42% for Rh6G, ~30% for C343, and 0% for C153. Therefore, the energy transfer efficiencies can be varied from 0% to 80% by the judicious selection of donor dyes. Since the energy transfer efficiency is strongly dependent on the distance between donor dyes and gold nanoparticles, partitioning of the donor dyes and acceptor nanoparticles into the same corona region results an effective dye to nanometal surface energy transfer and this efficient NSET process has been observed for C480, Rh6G, and C343 which are located in the same corona region together with the nanoparticles in the close proximity. Conversely, if donor and acceptor partition into two different region of large separation the extent of energy transfer will decrease as it has been observed for C153. Therefore, through the nano-encapsulation of the different fluorophore having different location inside P123 micelles, we have shown the corona region of P123 micelles as a perfect place for NSET and the core region as a barrier for NSET.

In order to get a semiquantitative picture, we have calculated the distance between donor and acceptor in such a complex system where there is a distribution of donor–acceptor distance instead of the single donor–acceptor distance, using both the simplified FRET and SET model. In spite of the complexity, such calculations of donor–acceptor distance have considerable potential for studies of multiple fluorophore organization in nanoparticles embedded micelles. In the analysis of FRET parameters, the Förster distance (R_0) i.e. the distance at which

RET is 50% efficient, can be calculated using the following equation

$$R_0 = 0.211[\kappa^2 n^{-4} Q_{\text{dye}} J(\lambda)]^{1/6} \quad (5)$$

where κ^2 is the orientation factor (2/3 in P123 micellar solution³²), n is the refractive index of the medium, Q_{dye} is the quantum yield of the donor dye in absence of acceptor, and $J(\lambda)$ is the spectral overlap integral between the absorption peak of acceptor and emission peak of donor. $J(\lambda)$ is calculated from the normalized fluorescence intensity ($F_D(\lambda)$) of the donor in the absence of acceptor and extinction coefficient of the acceptor $\epsilon_A(\lambda)$ using the following equation:¹³

$$J(\lambda) = \frac{\int_0^\infty F_D(\lambda) \epsilon_A(\lambda) \lambda^4 d\lambda}{\int_0^\infty F_D(\lambda) d\lambda} \quad (6)$$

The calculated Förster distances (R_0) are 198.3, 178.9, and 198.8 Å for Rh6G, C480, and C343, respectively. However in the successful application of FRET the Förster distance is typically in the range of 20–60 Å. Now, the distance (r) between molecular centers to the center of the nanoparticles can now be determined from the energy transfer efficiencies as

$$\phi_{\text{ET}} = \frac{1}{1 + \left(\frac{r}{R_0}\right)^6} \quad (7)$$

The estimated distances between donor and acceptor are 209.2, 143.4, and 228.9 Å for Rh6G, C480, and C343, respectively. These values are quite larger than the detection limit for FRET. It is well established that FRET is restricted to determine the distance between donor and acceptor up to the separation of only 80 Å and the sensitivity of FRET becomes too weak at large distance of separation. Thus FRET is not operational in this present system.^{47,65} Such nonoperational FRET behavior during the study of energy transfer from molecular donor to gold nanoparticles has been reported in number of previous reports.^{45–47,65}

However, in the case of studying energy transfer in Au–P123 hybrid systems of multiple donor–acceptor distances, more importance has been given on the fact that efficient energy transfer occurs whenever the donor and acceptor are in the same corona region, i.e., within the detection limit of NSET and less on the determination of precise donor–acceptor distance. It is well established that the steady state photo luminescence quenching along with the reduction in the emission lifetime is unambiguously attributed to the NSET process, which empirically exhibits $1/d^4$ distance dependence as it has been proven by several groups.^{12–14,21–23,45–47} The energy transfer processes strictly follow Fermi golden rule. Persson model³⁴ states that for a vibrating dipole located at a distance d above a metal surface, the damping rate i.e. the rate at which the vibrationally excited state decays to the vibrationally ground state with the scattering of an electron in the nearby metal to above the Fermi level can be obtained from the golden-rule formula. Interestingly, a difference in the distance dependence energy transfer rate is observed depending on the major or dominant contributing factor to the damping rate. For example, when surface contribution is the dominating factor, the damping rate follows $1/d^4$ distance dependence while for volume contribution it is $1/d^3$ distance dependent. This model further indicates that for a noble metal surface, the

Table 3. Nanometal Surface Energy Transfer (NSET) Parameters for Different Dye-Au Systems in Confined environment of P123 Nanohybrid

systems	λ_{emi}^{\max} (nm)	spectral overlap integral, $J(\lambda)$ ($M^{-1} \text{cm}^{-1} \text{nm}^4$)	quantum yield of donor, Φ_D^0	Förster distance, R_0 (Å)	D-A distance, r (Å)	d_0 (Å)	d (Å)
Rh6G in P123 micelles (5 wt %)	560		0.86				
Rh6G in Au-P123 nanohybrid	560	3.8×10^{18}	0.86	198.3	209.2	80.1	85.07
C-480 in P123 micelles (5 wt %)	468		0.84				
C480 in Au-P123 nanohybrid	468	2.1×10^{18}	0.84	178.9	143.4	67.4	48.4
C-343 in P123 micelles (5 wt %)	486		0.81				
C-343 in Au-P123 nanohybrid	476	4.06×10^{18}	0.81	198.8	228.9	70.5	87.1

surface damping is expected to dominate over volume damping if $d \leq 200$ Å and in that case the rate of surface energy transfer is expected to be $1/d^4$ distance dependent. Therefore, the equations of SET processes proposed by Persson, have been employed to determine the distance between donor and acceptor.³⁴ According to Persson model, the rate of surface energy transfer is given by

$$k_{et} = 0.3 \frac{\mu^2}{\hbar} \frac{\omega_{dye}}{\omega_F k_F d^4} \quad (8)$$

This can be expressed in more simplified form with measurable parameters:¹³

$$k_{\text{NSET}} = \frac{1}{\tau_D} \left(\frac{d_0}{d} \right)^4 \quad (9)$$

Hence, the quantum efficiency of SET process can thus be written as follows:

$$\Phi_{ET} = \frac{1}{1 + \left(\frac{d}{d_0} \right)^4} \quad (10)$$

where τ_D is the lifetime of the donor dye in the absence of acceptor, d is the distance between center of the molecular donor to the surface of NPs acceptor, and d_0 is the distance which is equivalent to Förster distance of FRET processes. The d_0 value is calculated theoretically using the NSET equation

$$d_0^{\text{NSET}} = \left(\frac{0.225 c^3 \Phi_{dye}}{\omega_{dye}^2 \omega_F k_F} \right)^{1/4} \quad (11)$$

The calculated distance parameters for the quenching of the excited state donor lifetime are given in Table 3. The distance between confined dyes and gold nanoparticles present in the corona region of micelles are 48.4, 85.07, and 87.1 Å for C480, Rh6G, and C343, respectively. Theoretically, Bagchi et al. have shown that at separation approximately between $d = a$, and $d = 4a$, the rate of energy transfer is in partial agreement with experimentally observed $1/d^4$ distance dependence. In our investigation the measured distances (d) ranges from 4.8 to 8.7 nm, while the average radius of nanoparticles (a) is ~4.5 nm. Since, under the present experimental condition all the measured distances fall within the range of a (4.5 nm) and $4a$ (18.0 nm) and therefore explain the validity of using $1/d^4$ distance dependence NSET equation. Here to understand the

real physical meaning of the calculated distances, we try to correlate the distances with average hydrodynamic radius of Au-P123 plasmonic nanohybrids obtained from DLS and TEM analysis. The relative distribution of fluorescent donor dyes in the corona region of P123 micelles plays an important role on the energy transfer efficiencies and thus has a great impact on the calculated distance parameters. Incorporation of nanoparticles into the surface cavities of P123 micelles, the corona region is substantially modified as observed from the change in micellar radius from ~9 nm of normal micelles to ~40 nm of nanoparticles loaded hybrid micelles. Now, the effective NSET from the donor–acceptor pair present in the same corona region of Au-P123 hybrid assemblies can be understood from the thickness of the modified corona region by subtracting the core radius (~4.8 nm) of normal micelles. The measured distances are smaller than the corona thickness of Au-P123 nanohybrids for efficient intramicellar energy transfer within the detection limit of NSET. In the micellar assemblies, multiple donor–acceptor distances are varying in a range depending on the distribution of the donor dyes inside micelles. In this situation the concentration of acceptors plays an important role because the acceptor concentration determines the donor–acceptor proximity. The shortest donor–acceptor distance arises from energy transfer between a pair of donor and acceptor present in the same hydrophilic corona region in close proximity. The longest distance corresponds to the acceptor at the corona and a donor in more toward the core. The ionic acceptors Rh6G, C343, and nonionic acceptor C480 preferentially reside at the same hydrophilic corona region together with metal nanoparticles hence efficient energy transfer occurs. However, C153 reside in the core region far apart from nanoparticles, which inhibit energy transfer. The average distance from the center of the core to the surface of the nanoparticles is ~30 nm considering the average radius of hybrid micellar assemblies is ~40 nm with surface embedded gold nanoparticles of average diameter ~8–10 nm. Such a large distance is effective barrier for both FRET and NSET. Due to this larger distance from core region to the surface of the nanoparticles, energy transfer is prohibited for the probe molecules which reside in the core region instead of the presence of good spectral overlap between fluorescence band of donor dyes and surface Plasmon resonance band of nanoparticles and this has been experimentally verified using C153.

CONCLUSION

In summary, we have successfully loaded Au NPs into the surface of micellar aggregates of P123 in a regular fashion and investigated NSET from embedded dye to the surface attached metal nanoparticles. A shortening of the average lifetime along with the significant steady state fluorescence quenching leading to NSET have been observed for Rh6G, C480, and C343 dyes which are preferentially located at the corona region of micelles in the close proximity of nanoparticles. Besides that a very good spectral overlap between fluorescence of donor dyes and the localized surface plasmon resonance band (LSPR) of the nanoparticles also validate the efficient NSET process. We have also demonstrated a comparative study on quenching efficiencies of different dyes having different location inside micelles in order to probe different regions of Au–P123 hybrid nanospheres. For the probe molecules like, C153 which reside preferably in the hydrophobic core region, far apart from the nanoparticles, the NSET process is prohibited instead of the presence of good spectral overlap. Furthermore, investigation on the microenvironments of the probe molecules in presence of nanoparticles reveals a modification of micelles loaded with Au NPs, that triggers the suitable anionic probe molecules to drag from the aqueous micellar phase to the interior of micelles as indicated from the significant blue shift of the emission maxima of C343 after the synthesis of nanoparticles on the micellar surface. On the basis of our all experimental findings we may conclude that such well-defined stable confined pluronic TBP based hybrid spherical assemblies with efficient loading of the fluorescent dye molecules and Au NPs will certainly be helpful to further explore its potential applicability in sensing and medicinal chemistry.

ASSOCIATED CONTENT

Supporting Information

Information on the change in the UV-visible absorption spectra for the synthesis of gold nanoparticles in dye loaded micelles of P123. This material is available free of charge via the Internet at <http://pubs.acs.org>.

AUTHOR INFORMATION

Corresponding Author

*E-mail: nilmoni@chem.iitkgp.ernet.in. Fax: 91-3222-255303.

Notes

The authors declare no competing financial interest.

ACKNOWLEDGMENTS

N.S. is thankful to Council of Scientific and Industrial Research (CSIR) and Board of Research in Nuclear Sciences (BRNS), Government of India, for generous research grants. S.M., C.G., V.G.R., and S.G. are thankful to CSIR for a research fellowship.

REFERENCES

- (1) Yokoyama, M. *Crit. Rev. Ther. Drug Carrier Syst* **1992**, *9*, 213–248.
- (2) Blanazs, A.; Armes, S. P.; Ryan, A. J. *Maromol. Rapid Commun.* **2009**, *30*, 267–277.
- (3) Svensson, B.; Olsson, U.; Alexandridis, P.; Mortensen, K. *Macromolecules* **1999**, *32*, 6725–6733.
- (4) Alexandridis, P.; Hatton, T. A. *Colloids Surf., A* **1995**, *96*, 1–46.
- (5) Das, D. K.; Das, A. K.; Mondal, T.; Mandal, A. K.; Bhattacharyya, K. *J. Phys. Chem. B* **2010**, *114*, 13159–13166.
- (6) Schillén, K.; Bryskhe, K.; Mel'nikova, Y. S. *Macromolecules* **1999**, *32*, 6885–6888.
- (7) Wang, X.; Kawanami, H.; Iwlam, N. M.; Chatterjee, M.; Yokoyama, T.; Ikushima, Y. *Chem. Commun.* **2008**, 4442–4444.
- (8) Hickey, R. J.; Haynes, A. S.; Kikkawa, J. M.; Park, S. *J. Am. Chem. Soc.* **2011**, *133*, 1517–1525.
- (9) Chen, J.; Zeng, F.; Wu, S.; Zhao, J.; Chen, Q.; Tong, Z. *Chem. Commun.* **2008**, 5580–5582.
- (10) Sasmal, D. K.; Mandal, A. K.; Mondal, T.; Bhattacharyya, K. *J. Phys. Chem. B* **2011**, *115*, 7781–7787.
- (11) Stryer, L.; Haugland, R. P. *Proc. Natl. Acad. Sci. U.S.A.* **1967**, *58*, 719–725.
- (12) Yun, C. S.; Javier, A.; Jennings, T.; Fisher, M.; Hira, S.; Peterson, S.; Hopkins, B.; Reich, N. O.; Strouse, G. F. *J. Am. Chem. Soc.* **2005**, *127*, 3115–3119.
- (13) Jennings, T. L.; Singh, M. P.; Strouse, G. F. *J. Am. Chem. Soc.* **2006**, *128*, 5462–5467.
- (14) Singh, M. P.; Strouse, G. F. *J. Am. Chem. Soc.* **2010**, *132*, 9383–9391.
- (15) Lakowicz, J. R. *Principles of Fluorescence Spectroscopy*, 3rd ed.; Springer: New York, 2006.
- (16) Seo, M.; Lee, T.; Kim, E.; Cho, Y. L.; Park, H.; Yoon, T.; Kim, H. *Anal. Chem.* **2011**, *83*, 8849–8854.
- (17) Dulkeith, E.; Ringler, M.; Klar, T. A.; Feldmann, J.; Munoz Javier, A.; Parak, W. J. *Nano Lett.* **2005**, *5*, 585–589.
- (18) Dubertret, B.; Calame, M.; Libchaber, A. *J. Nat. Biotechnol.* **2001**, *19*, 365–370.
- (19) Chen, Y.; O'Donoghue, M. B.; Huang, Y.; Kang, H.; Phillips, J. A.; Chen, X.; Estevez, M. C.; Yang, C. J.; Tan, W. *J. Am. Chem. Soc.* **2010**, *132*, 16559–16570.
- (20) Bene, L.; Szentesi, G.; Matyus, L.; Gaspar, R.; Damjanovich, S. *J. Mol. Recognit.* **2005**, *18*, 236–253.
- (21) Griffin, J.; Singh, A. K.; Senapati, D.; Rhodes, P.; Mitchell, K.; Robinson, B.; Yu, E.; Ray, P. C. *Chem.—Eur. J.* **2009**, *15*, 342–351.
- (22) Jennings, T. L.; Schlatterer, J. C.; Singh, M. P.; Greenbaum, N. L.; Strouse, G. F. *Nano Lett.* **2006**, *6*, 1318–1324.
- (23) Darbha, G. K.; Ray, A.; Ray, P. C. *ACS Nano* **2007**, *1*, 208–214.
- (24) Zheng, J.; Zhang, C.; Dickson, R. M. *Phys. Rev. Lett.* **2004**, *93*, 077402–077405.
- (25) Clapp, A. R.; Medintz, I. L.; Mauro, J. M.; Fisher, B. R.; Bawendi, M. G.; Mattoussi, H. *J. Am. Chem. Soc.* **2004**, *126*, 301–310.
- (26) Pons, T.; Medintz, I. L.; Wang, X.; English, D. S.; Mattoussi, H. *J. Am. Chem. Soc.* **2006**, *128*, 15324–15331.
- (27) Clapp, A. R.; Medintz, I. L.; Uyeda, H. T.; Fisher, B. R.; Goldman, E. R.; Bawendi, M. G.; Mattoussi, H. *J. Am. Chem. Soc.* **2005**, *127*, 18212–18221.
- (28) Peng, H.; Zhang, L.; Kjallman, T. H. M.; Soeller, C.; Sejdic, J. T. *J. Am. Chem. Soc.* **2007**, *129*, 3048–3049.
- (29) Yoo, S.; Bae, S. H.; Kim, K.; Sohn, B. *Soft Matter* **2009**, *5*, 2990–2996.
- (30) Clapp, A. R.; Medintz, I. L.; Fisher, B. R.; Anderson, G. P.; Mattoussi, H. *J. Am. Chem. Soc.* **2005**, *127*, 1242–1250.
- (31) Malicka, J.; Gryzynski, I.; Kusba, J.; Lakowicz, J. R. *Biopolymers* **2003**, *70*, 595–603.
- (32) Ghosh, S.; Dey, S.; Adhikari, A.; Mandal, U.; Bhattacharyya, K. *J. Phys. Chem. B* **2007**, *111*, 7085–7091.
- (33) Seth, D.; Chakraborty, A.; Setu, P.; Chakraborty, D.; Sarkar, N. *J. Phys. Chem. B* **2005**, *109*, 12080–12085.
- (34) Persson, B. N. J.; Lang, N. D. *Phys. Rev. B* **1982**, *26*, 5409–5415.
- (35) Lakowicz, J. R. *Anal. Biochem.* **2005**, *337*, 171–194.
- (36) Lakowicz, J. R. *Anal. Biochem.* **2001**, *298*, 1–24.
- (37) Jain, P. K.; Lee, K. S.; El-Sayed, I. H.; El-Sayed, M. A. *J. Phys. Chem. B* **2006**, *110*, 7238–7248.
- (38) Mie, G. *Ann. Phys. (Leipzig)* **1908**, *25*, 377–445.
- (39) Draine, B. T.; Flatau, P. J. *J. Opt. Soc. Am. A* **1994**, *11*, 1491–1499.
- (40) Saini, S.; Shenoy, V. B.; Bagchi, B. *J. Phys. Chem. C* **2008**, *112*, 6299–6306.
- (41) Saini, S.; Srinivas, G.; Bagchi, B. *J. Phys. Chem. B* **2009**, *113*, 1817–1832.

- (42) Bhowmick, S.; Saini, S.; Shenoy, V. B.; Bagchi, B. *J. Chem. Phys.* **2006**, *125*, 181102–181107.
- (43) Kelly, K. L.; Coronado, E.; Zhao, L. L.; Schatz, G. C. *J. Phys. Chem. B* **2003**, *107*, 668–677.
- (44) Swathi, R. S.; Sebastian, K. L. *J. Chem. Phys.* **2007**, *126*, 234701–234705.
- (45) Sen, T.; Jana, S.; Koner, S.; Patra, A. *J. Phys. Chem. C* **2010**, *114*, 19667–19672.
- (46) Sen, T.; Halder, K. K.; Patra, A. *J. Phys. Chem. C* **2010**, *114*, 11409–11413.
- (47) Sen, T.; Halder, K. K.; Patra, A. *J. Phys. Chem. C* **2008**, *112*, 17945–17951.
- (48) Khullar, P.; Mahal, A.; Singh, V.; Banipal, T. S.; Kaur, G.; Bakshi, M. S. *Langmuir* **2010**, *26*, 11363–11371.
- (49) Khullar, P.; Singh, V.; Mahal, A.; Kaur, H.; Singh, V.; Banipal, T. S.; Kaur, G.; Bakshi, M. S. *J. Phys. Chem. C* **2011**, *115*, 10442–10454.
- (50) Hu, J.; Qian, Y.; Wang, X.; Liu, T.; Liu, S. *J. Phys. Chem. C* **2011**, 10.1021/la203992q
- (51) Sperling, R. A.; Gil, P. R.; Zang, F.; Zanella, M.; Parak, W. J. *Chem. Soc. Rev.* **2008**, *37*, 1896–1908.
- (52) Kim, D.; Jeong, Y. Y.; Jon, S. *ACS Nano* **2010**, *4*, 3689–3696.
- (53) Luo, Y.; Shiao, Y.; Huang, Y. *ACS Nano* **2011**, *5*, 7796–7804.
- (54) Adams, M. L.; Lavasanifar, A.; Kwon, G. S. *J. Pharm. Sci.* **2003**, *92*, 1343–1355.
- (55) Meng, F.; Zhong, Z. *J. Phys. Chem. Lett.* **2011**, *2*, 1533–1539.
- (56) Raino, G.; Stoferle, T.; Park, C.; Kim, H.; Topuria, T.; Rice, P. M.; Chin, I.; Miller, R.; Mahrt, R. F. *ACS Nano* **2011**, *5*, 3536–3541.
- (57) Yoo, S. I.; Bae, S. H.; Kim, K.; Sohn, B. *Soft Matter* **2009**, *5*, 2990–2996.
- (58) Grant, C. D.; Steege, K. E.; Bunagan, M. R.; Castner, E. W. Jr. *J. Phys. Chem. B* **2005**, *109*, 22273–22284.
- (59) Grant, C. D.; DeRitter, M. R.; Steege, K. E.; Fadeeva, T. A.; Castner, E. W. Jr. *Langmuir* **2005**, *21*, 1745–1752.
- (60) Sahu, K.; Ghosh, S.; Mondal, S. K.; Ghosh, B. C.; Sen, P.; Roy, D.; Bhattacharyya, K. *J. Chem. Phys.* **2006**, *125*, 044714–044721.
- (61) Karthikeyan, B. *J. App. Phys.* **2010**, *108*, 084311–084315.
- (62) Kumbhakar, M.; Goel, T.; Nath, S.; Mukherjee, T.; Pal, H. *J. Phys. Chem. B* **2006**, *110*, 25646–25655.
- (63) Singh, P. K.; Satpati, A. K.; Kumbhakar, M.; Pal, H.; Nath, S. *J. Phys. Chem. B* **2008**, *112*, 11447–11450.
- (64) Singh, P. K.; Kumbhakar, M.; Pal, H.; Nath, S. *J. Phys. Chem. B* **2009**, *113*, 1353–1359.
- (65) Saraswat, S.; Desiraju, A.; Zheng, D.; Guo, L.; Lu, H. P.; Bigioni, T. P.; Isailovic, D. *J. Phys. Chem. C* **2011**, *115*, 17587–17593.
- (66) Haiss, W.; Thanh, N. T. K.; Aveyard, J.; Fering, D. G. *Anal. Chem.* **2007**, *79*, 4215–4221.
- (67) Jones, G. II; Jackson, W. R.; Choi, C.-Y.; Bergmark, W. R. *J. Phys. Chem.* **1985**, *89*, 294–300.
- (68) Magde, D.; Wong, R.; Seybold, P. G. *Photochem. Photobiol.* **2002**, *75*, 327–334.
- (69) Reynolds, G. A.; Drexhage, K. H. *Opt. Commun.* **1975**, *13*, 222–225.
- (70) Ganguly, R.; Kumbhakar, M.; Aswal, V. K. *J. Phys. Chem. B* **2009**, *113*, 9441–9446.
- (71) Zhong, Z.; Lee, H.; Shena, S.; Gedanken, A. *Soft Matter* **2009**, *5*, 2558–2562.
- (72) Sakai, T.; Alexandridis, P. *Langmuir* **2004**, *20*, 8426–8430.
- (73) Lim, S. Y.; Kim, J. H.; Lee, J. S.; Park, C. B. *Langmuir* **2009**, *25*, 13302–13305.
- (74) Setua, P.; Pramanik, R.; Sarkar, S.; Seth, D.; Sarkar, N. *J. Phys. Chem. B* **2009**, *113*, 5677–5680.